Available online at www.sciencedirect.com

ScienceDirect

Ceramics International 40 (2014) 4541–4551

CERAMICS INTERNATIONAL

www.elsevier.com/locate/ceramint

Reduction behaviors and catalytic properties for methanol steam reforming of Cu-based spinel compounds CuX_2O_4 (X=Fe, Mn, Al, La)

Yung-Han Huang[a], Sea-Fue Wang[a,*], An-Pang Tsai[b], Satoshi Kameoka[b]

[a]Department of Materials and Mineral Resources Engineering, National Taipei University of Technology 1, Sec. 3, Chung-Hsiao E. Road, Taipei 10608, Taiwan, ROC
[b]Institute of Multidisciplinary Research for Advanced Materials, Tohoku University, 2-1-1 Katahira, Aoba-ku, Sendai 980-8577, Japan

Received 20 July 2013; accepted 30 August 2013
Available online 19 September 2013

Abstract

In this study, various Cu-based spinel compounds, i.e., $CuFe_2O_4$, $CuMn_2O_4$, $CuAl_2O_4$ and $CuLa_2O_4$, were fabricated by a solid-state reaction method. Reduction behaviors and morphological changes of these materials have been characterized by H_2 temperature-programmed reduction (H_2-TPR), X-ray diffraction (XRD), Scanning electron microscopy (SEM), and transmission electron microscopy (TEM). Moreover, the catalytic properties for steam reforming of methanol (SRM) of these Cu-based spinel compounds were investigated. H_2-TPR results indicated that the reducibility of Cu-based spinel compounds was strongly dependent on the B-site component while the $CuFe_2O_4$ catalyst revealed the lowest reduction temperature (190 °C), followed respectively by $CuAl_2O_4$ (267 °C), $CuMn_2O_4$ (270 °C), and $CuLa_2O_4$ (326 °C). The reduced $CuAl_2O_4$ catalyst demonstrated the best performance in terms of catalytic activity. Based on the SEM and XRD results, pulverization of the $CuAl_2O_4$ particles due to gas evolution and a high concentration of nanosized Cu particles (≈ 50.9 nm) precipitated on the surfaces of the Al_2O_3 support were observed after reduction at 360 °C in H_2. The BET surface area of the $CuAl_2O_4$ catalyst escalated from 5.5 to 13.2 m^2/g. Reduction of Cu-based spinel ferrites appear to be a potential synthesis route for preparing a catalyst with high catalytic activity and thermal stability. The catalytic performance of these copper-oxide composites was superior to those of conventional copper catalysts.

Keywords: Catalyst; Steam reforming of methanol (SRM); Cu-based spinel compounds

1. Introduction

Cu-based catalysts demonstrate promising high activity and selectivity for various reactions such as steam reforming of methanol (SRM) and water–gas shift reaction [6,9,11,13]. Highly dispersed Cu catalysts are traditionally prepared via impregnation, co-precipitation, and other methods [1–8]. However, difficulty of fine dispersion of Cu particles on supports and poor thermal stability remain the major drawbacks. Recently, perovskite- and spinel-type oxides have been identified as quite effective catalysis materials. As reported in several studies, Cu-based catalysts prepared by reduction treatment of spinel oxides (especially the Cu/MnO system) showed high activity in water–gas shift reaction [9–11]. According to Papavasiliou et al. [12,13], Cu–MnO catalysts prepared via combustion method revealed good CO oxidation and reforming reactions. Tsai et al. prepared Cu catalysts from mixed oxides based on the metallurgical methodology by which Cu catalysts were fabricated directly from $CuCrO_2$ with a delafossite structure and $CuFe_2O_4$ with a spinel structure [14–15]. High catalytic performance and good thermal stability of the composite structure comprising nano-scale Cu particles homogeneously dispersed in the porous Cr_2O_3 and Fe_3O_4 matrixes were generated by the reductive decomposition of $CuCrO_2$ and $CuFe_2O_4$ [14–15]. However, reduction behaviors and morphological changes for different spinel oxide compounds have not been examined systematically.

In this study, various Cu-based spinel compounds ($CuMn_2O_4$, $CuFe_2O_4$, $CuAl_2O_4$ and $CuLa_2O_4$) were fabricated by the solid-state reaction technique. Reduction behaviors including morphological changes and catalytic properties of the Cu-based spinel compounds were systematically investigated. The microstructure and catalytic performance for SRM reaction and the phase structure of the compounds after reduction treatment were

*Corresponding author. Tel.: +886 2 2771 2171x2735; fax: +886 2 2731 7185.
E-mail addresses: sfwang@ntut.edu.tw, seafuewang@yahoo.com (S.-F. Wang).

0272-8842/$ - see front matter © 2013 Elsevier Ltd and Techna Group S.r.l. All rights reserved.
http://dx.doi.org/10.1016/j.ceramint.2013.08.130

characterized and discussed based on the results of X-ray diffraction (XRD), temperature program reduction (TPR), scanning electron microscopy (SEM), transmission electron microscopy (TEM), and catalytic performance of SRM reaction.

2. Experimental procedure

In this study, Cu-based spinel compounds were prepared using the solid-state reaction technique. Highly pure CuO (Nikko Rica Corporation, Reagent grade), α-Fe_2O_3 (Voestalpine Company, Reagent grade), La_2O_3 (SHOWA, Reagent grade), α-Al_2O_3 (SHOWA, Reagent grade), and Mn_2O_3 (STREM, Reagent grade) were used as raw materials. Stoichiometric mixtures of the powders were milled in methyl alcohol solution using polyethylene jars and zirconia balls for 24 h and then dried at 90 °C in an oven for overnight. After drying, the powders were calcined in air at 1000 °C for 4 h and subsequently re-milled in methyl alcohol for 24 h.

Phase identification of the powders was performed using X-ray diffraction (Mac Science, M03XHF22). To record the quantity of H_2 consumption caused by the reduction reaction of spinel compounds and H_2 during heating, H_2 temperature-programmed reduction (H_2-TPR) measurements were conducted using 15 mg catalyst from room temperature to 800 °C at a heating rate of 10 °C/min with a flow of 5% H_2/Ar (30 mL/min). Surface area determination of particles was performed using BET analysis from N_2 adsorption–desorption isotherms at 77 K (BELSORP-mini, BEL JAPAN, Inc.). SEM (Hitachi, SU8000) technique was used to determine the morphology and the nature of the agglomerates in the catalyst. Detailed microstructure was obtained in a JEOL 2010 microscope installed with an energy filter at an operating voltage of 200 kV. The Cu^0 surface area was calculated assuming a molar stoichiometry of N_2O/Cu(s)=0.5 from the amount of N_2O consumed in the reaction, where Cu(s) denotes a surface copper atom with the surface density of copper metal set at an average 1.46×10^{19} copper atoms/m^2 [16–17,30].

$$2Cu + N_2O \rightarrow Cu_2O + N_2 \quad (1)$$

Steam reforming of methanol (SRM:$CH_3OH + H_2O \rightarrow 3H_2 + CO_2$) reactions took place in a conventional flow reactor at 100 kPa. The Cu-based spinel compounds were reduced in a hydrogen atmosphere at 240–600 °C prior to reaction. Inlet partial pressures of methanol, water, and nitrogen (used as a dilutant) read 35.5, 52.7, and 13.2 kPa, respectively (LHSV of CH_3OH/H_2O mixture: 25 h^{-1}, CH_3OH/H_2O=2/3). The reaction products were analyzed by an on-line gas chromatograph (Shimadzu, GC 14 A) equipped with a Shincarbon column (H_2, CO, CO_2, and CH_4) under Ar carrier gas. The data from GC equipment were recorded when the reaction was maintained at a stable state after 30 min at each temperature. The catalytic activity for the SRM reaction was evaluated in term of H_2 production rate (mol min^{-1} Cu-site^{-1}). In this study, H_2, CO_2 and CO were detected as products in the SRM. Methanol conversion and selectivity to CO and CO_2 gas are defined as

$$\text{Methanol conversion}(\%) = \frac{F_{CO} + F_{CO_2}}{F_{\text{Methanol}}} \times 100\% \quad (2)$$

$$\text{CO Selectivity}(\%) = \frac{F_{CO}}{F_{CO_2} + F_{CO}} \quad (3)$$

and

$$CO_2 \text{ Selectivity}(\%) = \frac{F_{CO_2}}{F_{CO_2} + F_{CO}} \quad (4)$$

3. Results and discussion

3.1. Reduction behaviors of various Cu-based spinel compounds

The Cu-based spinel compounds prepared in this study were confirmed by the XRD patterns shown in Fig. 1(a), after calcination at 1000 °C in air for 4 h. The XRD pattern of the $CuMn_2O_4$ sample was identified as a cubic structure (JCPDS card#74-2422, a=8.308 Å). A small amount of Mn_3O_4 was also detected in the pattern, a finding consistent with those reported in the literature [10,11]. The peaks responsible for the tetragonal-structured $CuFe_2O_4$ were recognized by JCPDS card #34-0425 (a=5.821 Å, c=8.703 Å) and appeared to agree with those shown in previous studies [14,18]. The experimental results showed that the compound formed after the mixture of CuO and α-Al_2O_3 calcined at 1000 °C could be assigned to the copper–alumina spinel $CuAl_2O_4$ (JCPDS card#33-0448; cubic; a=8.075 Å). The $CuLa_2O_4$ sample was confirmed by JCPDS card #72-1709 (a=5.358 Å, b=5.409 Å, and c=13.145 Å) as an orthorhombic structure. H_2-TPR measurements were then carried out on the Cu-based spinel compounds; the characteristic reduction behaviors displayed in Fig. 2 reveal that the quantities of H_2 consumption versus temperature, associated with the reduction process, of these four spinel compounds were significantly different. It is apparent that the Cu-based spinel compounds were more difficult to be reduced than CuO. Reducibility of the Cu-based spinels was obviously dependent on the B-site component, such as Mn, Fe, or La. Reduction of the $CuFe_2O_4$ powders started at the lowest temperature (190 °C) while that of the $CuLa_2O_4$ powders at the highest (326 °C). The reaction of the $CuMn_2O_4$ sample occurred at a narrow temperature range; on the other hand, the $CuFe_2O_4$, $CuAl_2O_4$ and $CuLa_2O_4$ compounds completed the reactions over a broad temperature range. During heating, the $CuMn_2O_4$ sample exhibited a sharp reduction peak initiated around 270 °C, which might be ascribed to the reduction of $CuMn_2O_4$ to metallic Cu, Cu_2O and MnO, as shown in Fig. 1(b). The coexistence of Cu and Cu_2O after reduction was also observed in the study of Tanaka et al. [9]. All copper oxides were reduced to Cu as the temperature reached above 400 °C, while no peak was observed in the higher temperature range, revealing that MnO was highly stable under reducing condition up to 800 °C and the final products of Cu and MnO were retained,

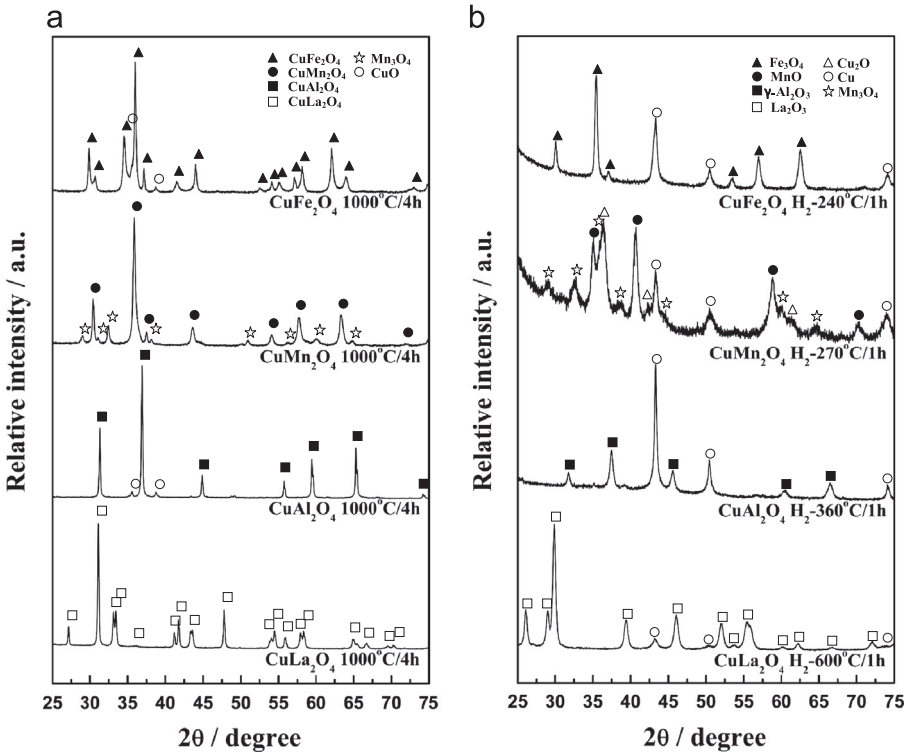

Fig. 1. XRD patterns of the Cu-based spinel compounds; (a) before and (b) after H_2 reduction at different temperatures.

according to the reaction path below:

$$CuMn_2O_4 \rightarrow Cu^* + Cu_2O + MnO \rightarrow Cu^* + MnO \quad (5)$$

Two broadened peaks were found located at around 240 °C and 600 °C for the $CuFe_2O_4$ powders during heating in the hydrogen atmosphere. The peak appearing at a lower temperature was attributed to the reduction of CuO to Cu in the spinel lattice, triggered at 190 °C and reaching its maximum at 273 °C. The subsequent peak corresponded to the reduction of Fe_3O_4 to Fe whose maximum rate occurred at 618 °C. It is hard to draw a clear boundary between these two reduction steps. The reaction sequence of the reductions followed the path shown below:

$$CuFe_2O_4 \rightarrow Cu^* + Fe_3O_4 \rightarrow Cu^* + Fe^* \quad (6)$$

The Cu and Fe phases were immiscible based on the phase diagram and the XRD results obtained, leaving mixture of pure metallic Fe and Cu, which is in agreement with those reported in the literature [14,18]. Two peaks were observed in the H_2-TPR profile of $CuAl_2O_4$. The first one, initiated at ≈220 °C and maximized at 268 °C, corresponded to the reduction of residue CuO or surface CuO to Cu, and the second peak started at a temperature overlapping with that of the former peak and rose to 449 °C due to the reduction of $CuAl_2O_4$ to Cu and γ-Al_2O_3 phases [19,20] because CuO peaks could be observed at around 35–40° and 47° in $CuAl_2O_4$ of Fig. 1(a).

$$CuAl_2O_4 \rightarrow Cu^* + \gamma - Al_2O_3 \quad (7)$$

In the case of the $CuLa_2O_4$ compound, a board peak with a shoulder ranging from 300 to 600 °C was detected. Also

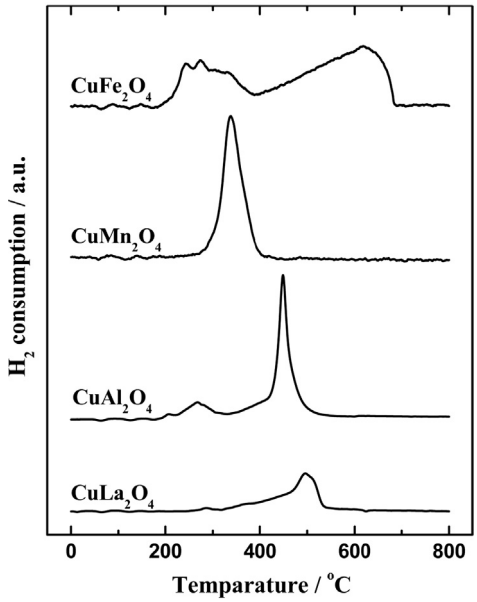

Fig. 2. TPR profiles of the Cu-based spinel compounds; TPR conditions: heat rate 10 °C/min in 5% H_2/Ar.

observed was measureable reduction recorded at 326 °C, maximized at 496 °C, and corresponding to the formation of Cu and La_2O_3.

$$CuLa_2O_4 \rightarrow Cu^* + La_2O_3 \quad (8)$$

Based on the H_2-TPR results, the $CuFe_2O_4$, $CuMn_2O_4$, $CuAl_2O_4$ and $CuLa_2O_4$ compounds were reduced respectively

at 240, 270, 360, and 600 °C in hydrogen atmosphere for 1 h, in order to characterize reduction behaviors and morphological changes. The XRD diffraction patterns for the compounds after reduction are shown in Fig. 1(b). As expected, $CuMn_2O_4$ was reduced and decomposed to Cu, Cu_2O and MnO; $CuFe_2O_4$ to Cu and Fe_3O_4; $CuAl_2O_4$ to Cu and γ-Al_2O_3, and $CuLa_2O_4$ to Cu and La_2O_3. SEM micrographs of the spinel $CuMn_2O_4$ compound before and after reduction in H_2 atmosphere are presented in Fig. 3. Before reduction, the $CuMn_2O_4$ compound revealed a granular morphology with smooth surfaces [Fig. 3 (a) and (b)], whereas, after H_2 reduction treatment at 270 °C, pulverization was observed in the $CuMn_2O_4$ particles due to gas evolution and a high concentration of nanosized Cu particles precipitated on the surfaces of the oxide support [Fig. 3(c) and (d)]. As the reduction temperature was raised to 400 °C, the morphology was detected to evolve into a nanoporous structure. Fig. 4 displays the TEM bright-field image (a) together with element mapping for Cu (b) and Mn (c) for the $CuMn_2O_4$ after H_2 reduction at 270 °C. Cu particles with sizes around 10–20 nm are visible in the images. According to element mapping, the distribution of Mn is slightly more homogeneous than that of Cu, indicating that MnO acts as a matrix or support. The porous structure was observed in H_2-reduced $CuFe_2O_4$ but not in the rest [14,18,23–26].

For the $CuFe_2O_4$ powders before H_2 reduction, a granular morphology with smooth surfaces can be clearly observed in the SEM micrographs presented in Fig. 5(a) and (b). After reduction in H_2 atmosphere at 240 °C, large cracks were noted, as well as pulverization of the powders, presence of Cu particles approximately 10 nm to 30 nm distributed on the particle surfaces, and formation of nanopores with sizes similar to those of Cu particles [Fig. 5(c) and (d).], all in accord with the results reported by Kameoka et al. In Fig. 6(a) and (b) that show the SEM micrographs of $CuAl_2O_4$ before reduction, granular $CuAl_2O_4$ particles in the range of 150–300 nm can be observed. After reduction, a huge amount of Cu particles with sizes ranging from 30 nm to 70 nm were formed on the γ-Al_2O_3 surfaces [Fig. 6(c) and (d)]. According to the SEM images in Fig. 7(a) and (b), the $CuLa_2O_4$ sample before H_2 reduction appeared in the form of granular powders with glossy surfaces. Larger cracks and some tiny Cu particles about 20 nm deposited on the powder surfaces were observed after reduction in H_2 atmosphere at 600 °C [Fig. 7(c) and (d)]. The change in the surface structure of the $CuLa_2O_4$ powders was trivial, and the number of Cu particles considerably lower as compared to those in the $CuMn_2O_4$ and $CuFe_2O_4$, $CuAl_2O_4$ powders, though reduction occurred at a much higher temperature.

Table 1 summarizes the results of the physicochemical properties of the $CuFe_2O_4$, $CuMn_2O_4$, $CuAl_2O_4$, and $CuLa_2O_4$ powders before and after reduction by hydrogen at 240, 270, 360, and 600 °C, respectively. Crystallite sizes of the copper particles estimated from XRD peaks are also summarized in Table 1. The surface areas increased from 2.4 to 6.6 m^2/g for $CuMn_2O_4$, from 2.2 to 5.0 m^2/g for $CuFe_2O_4$, and from 5.5 to 13.2 m^2/g for $CuAl_2O_4$ after H_2 reduction, escalating respectively by 2.8, 2.3 and 2.4 times. Different from these three cases, the surface area of the $CuLa_2O_4$ powders reported no significant growth, reading 0.95 m^2/g before and 1.3 m^2/g after reduction treatment. SEM results confirmed the changes in the surface areas of the Cu-based spinel compounds after reduction. The increase in the surface area of $CuMn_2O_4$ was mainly due to the precipitation of a huge number of Cu particles and partly due to the pulverization of the

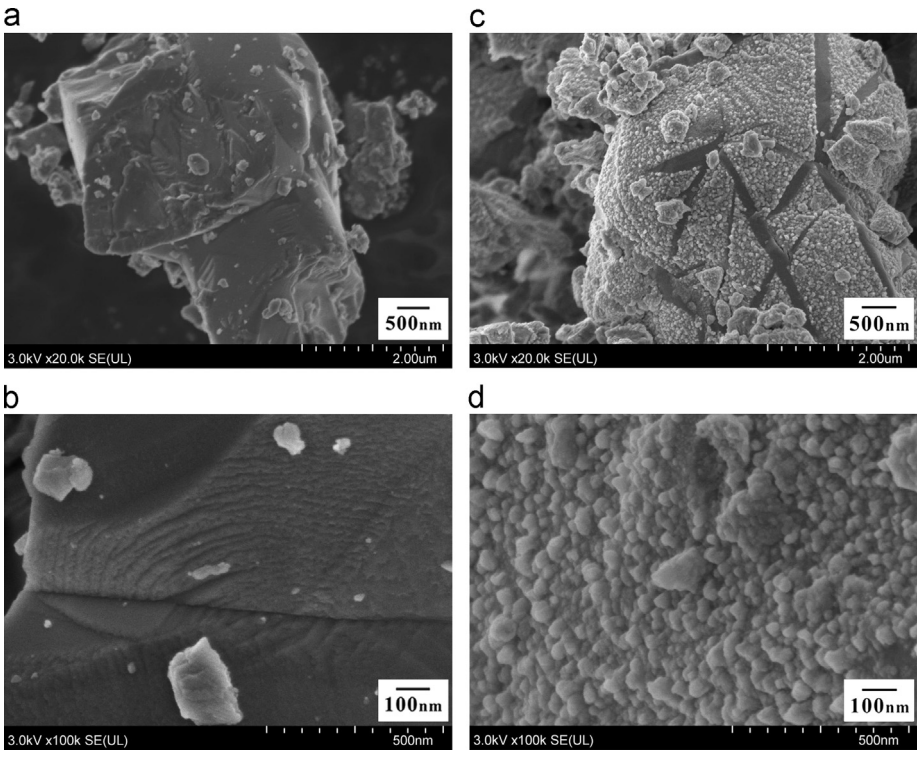

Fig. 3. SEM micrographs of the $CuMn_2O_4$ powders before [(a) and (b)] and after [(c) and (d)] reduction in H_2 atmosphere at 270 °C.

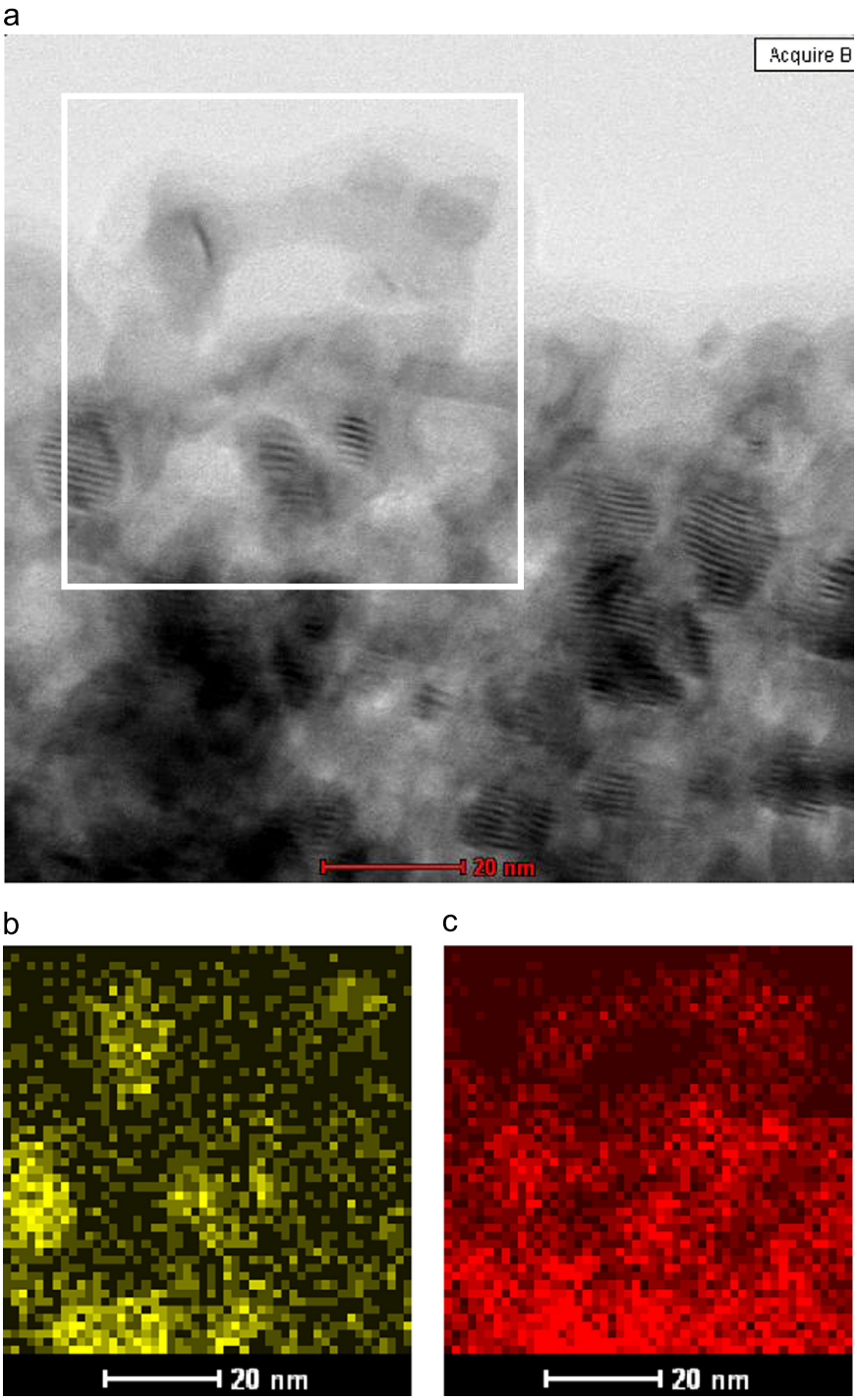

Fig. 4. TEM bright-field image (a) together with element mapping for Cu (b) and Mn (c) for the $CuMn_2O_4$ powders after H_2 reduction at 270 °C.

powders, while that of the $CuFe_2O_4$ powders was caused primarily by the precipitation of Cu particles and the generation of nanopores and partly by the pulverization of the powders. A Small amount of Cu on the glossy surfaces of $CuLa_2O_4$ after reduction by H_2 [Fig. 7(c) and (d)] led to little change in the surface area. The Cu surface area of a catalyst is often almost linearly related to its total BET surface area [21]. The BET surface area (13.2 m^2/g) of the $CuAl_2O_4$ powders emerged to be larger than those of the $CuFe_2O_4$ powders (5.0 m^2/g) and $CuMn_2O_4$ powders (6.6 m^2/g). The surface area of $CuLa_2O_4$ after reduction (1.3 m^2/g) was relatively small in comparison with those of $CuMn_2O_4$, $CuFe_2O_4$ and $CuAl_2O_4$.

3.2. Catalytic performance of copper-oxide composites obtained by reduction of various Cu-based spinel compounds

Fig. 8(a) illustrates the rates of H_2 production as a function of reaction temperature in the SRM reaction over Cu-based

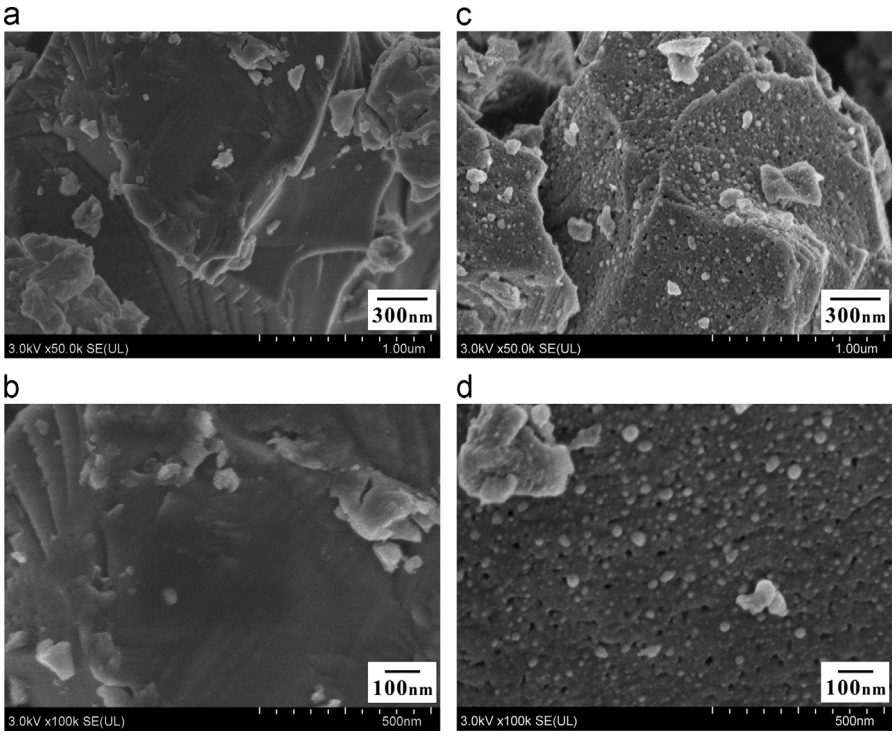

Fig. 5. SEM micrographs of the $CuFe_2O_4$ powders before [(a) and (b)] and after [(c) and (d)] reduction in H_2 atmosphere at 240 °C.

spinel compounds after H_2 reduction. In all cases, H_2 production rate increased as the reaction temperature rose from 240 to 320 °C. As indicated by the results, the $CuAl_2O_4$ sample reported the highest rate of H_2 production ranging from 13 to 52 (mol min^{-1} Cu-site^{-1}) for the SRM reaction, followed respectively by the $CuLa_2O_4$ sample (from 7 to 35 mol min^{-1} Cu-site^{-1}), the $CuFe_2O_4$ sample (from 6 to 23 mol min^{-1} Cu-site^{-1}), and the $CuMn_2O_4$ sample (from 5 to 12 mol min^{-1} Cu-site^{-1}). The catalytic performance of the Cu-based spinel compounds were also compared with that of a commercial Cu/Zn/Al reforming catalyst and CuO compound under identical reaction conditions. Catalysts with a higher catalytic activity appeared to have a lower reduction temperature, attributable to the smaller sizes of Cu particles due to thermodynamic instability [21]. In this study, though the $CuFe_2O_4$ sample could be reduced at a lower temperature (190 °C) and the Cu particles (29.4 nm) on the Fe_3O_4 support were smaller as compared to those observed in the $CuMn_2O_4$ (270 °C; 46.2 nm) and $CuAl_2O_4$ (360 °C; 50.9 nm) samples, the latter revealed a higher catalytic activity solely due to the larger surface area. The SRM activity of the $CuFe_2O_4$ sample obtained in this study was similar to the one reported by Kameoka et al., indicating that the rate of H_2 production for $CuFe_2O_4$ after reduction is one order higher than those of the Cu/Zn/Al commercial catalyst (S_{BET} = 78 m^2/g), physically mixed CuO + Fe_2O_3, and CuO, in terms of real rate [ml/min. m^2-cat] [14,22]. Apparently, the structure of the oxide supports of the Cu particles and the synthesis route of the catalysts play important roles in catalytic activity. The exact mechanism responsible for the high catalytic activity of the Cu-based spinel compounds remains an open question for further investigations.

Methanol conversion of the commercial catalyst and that of CuO are respectively the highest and lowest in these catalyst at 240 °C. Although the commercial catalyst apparently exhibits the highest activities, its rate of H_2 production with respect to the specific rate (mol s^{-1} Cu-site^{-1}) is lower than those of the spinel $CuAl_2O_4$, $CuFe_2O_4$ and $CuLa_2O_4$ catalysts. These results indicate that the copper particles generated from the spinel oxides show much higher catalytic performance than those from conventional catalysts.

Table 2 shows the Cu dispersions of the spinel catalysts and their TOF (turnover frequency) values for SRM at 280 °C. Interestingly, $CuAl_2O_4$ and $CuLa_2O_4$ surpassed the other catalysts in terms of catalytic TOF for SRM. The Cu dispersions and the TOFs were estimated based on the N_2O titration method [16–17,30]. It is clear that the dispersion of Cu follows the order of COM > $CuMn_2O_4$ > $CuFe_2O_4$ > $CuAl_2O_4$ > $CuLa_2O_4$ > CuO. Despite its low Cu surface area of 14.6 m^2/g-Cu, the $CuAl_2O_4$ catalysts had a high TOF at 280 °C which was comparable to the other Cu-based catalysts at the same temperature. The value of TOF over the $CuAl_2O_4$ compound was about ~6.6 times higher than that of the commercial catalyst. The order of TOFs emerges to be $CuAl_2O_4$ > $CuLa_2O_4$ > $CuFe_2O_4$ > $CuMn_2O_4$ > COM > CuO. TOFs of $CuAl_2O_4$ and $CuLa_2O_4$ are higher than those of $CuFe_2O_4$ and $CuMn_2O_4$. These results indicate that the optimum states of copper particles for high catalytic performance exist in their copper-oxides composites.

It is well known that the particle sizes of copper and the interaction of copper particles with oxides affect both surface structure and electronic properties. Several studies have confirmed the role of copper particles in close contact with oxides in increasing the binding strength of intermediates and decreasing

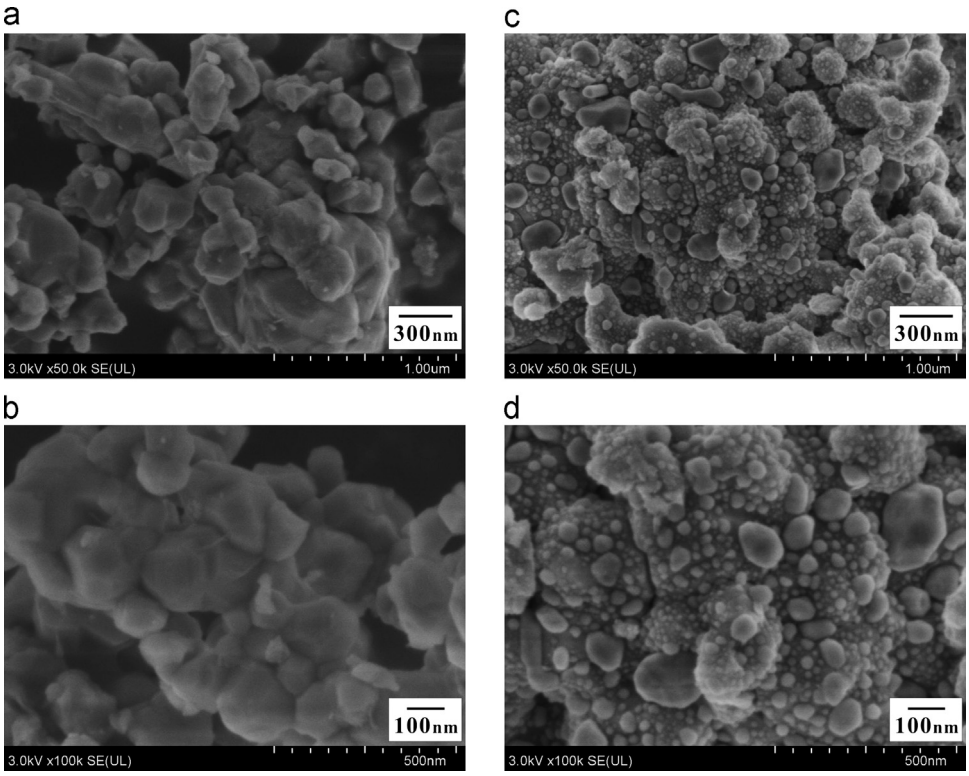

Fig. 6. SEM micrographs of the $CuAl_2O_4$ powders before [(a) and (b)] and after [(c) and (d)] reduction in H_2 atmosphere at 360 °C.

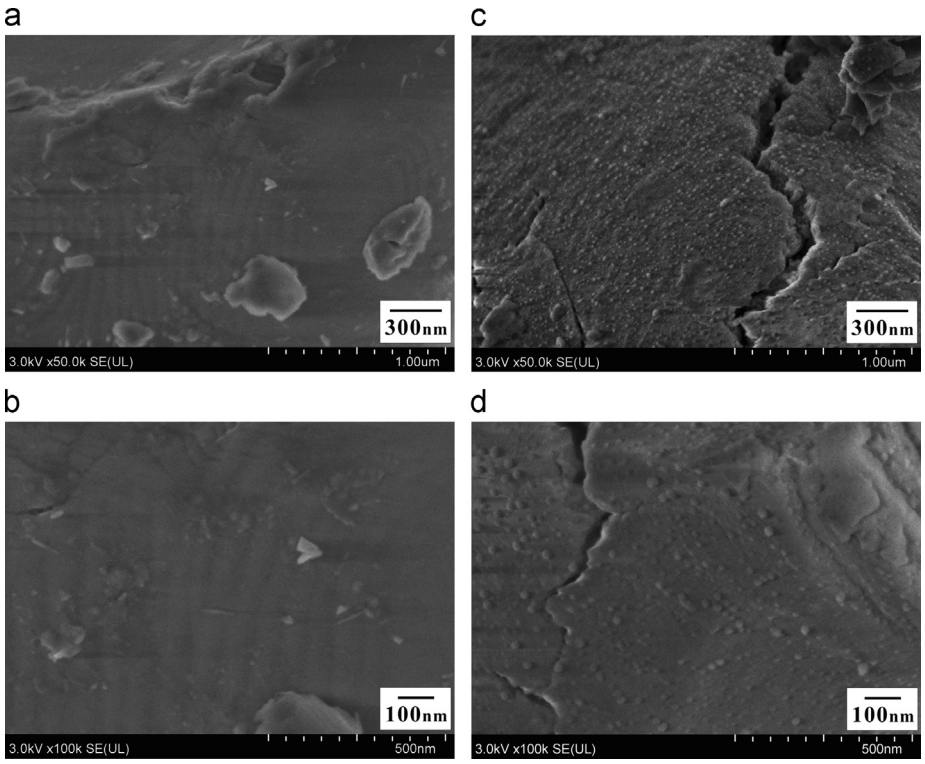

Fig. 7. SEM micrographs of the $CuLa_2O_4$ powders before [(a) and (b)] and after [(c) and (d)] reduction in H_2 atmosphere at 600 °C.

reaction barriers [13,18,25,29] Therefore, the states of copper particles generated from $CuAl_2O_4$ and $CuLa_2O_4$ seem to be suitable for SRM.

Fig. 9 displays the selectivity of CO and CO_2 versus reaction temperature of the Cu-based spinel compounds after the SRM reaction that increases with the rise in reaction

Table 1
Physicochemical properties of the $CuFe_2O_4$, $CuMn_2O_4$, $CuAl_2O_4$, $CuLa_2O_4$ powders before and after reduction.

Catalyst	Cu weight percent [wt %]	Reduction temperature[a] [°C]	Surface area [m^2/g]		Cu particles	
			Before reduction	After reduction	Crystallite size from XRD[b] [nm]	Particle size from SEM [nm]
$CuFe_2O_4$	26.6	240	2.2	5.0	16.6	29.4
$CuMn_2O_4$	26.8	270	2.4	6.6	16.8	46.2
$CuAl_2O_4$	35.0	360	5.5	13.2	27.4	50.9
$CuLa_2O_4$	15.7	600	0.95	1.3	12.1	21.4

[a]Reduction treatment at H_2 atmosphere.
[b]Cu crystalline size calculated from the XRD patterns after H_2 reduction using Scherrer equation for the Cu (111) reflection.

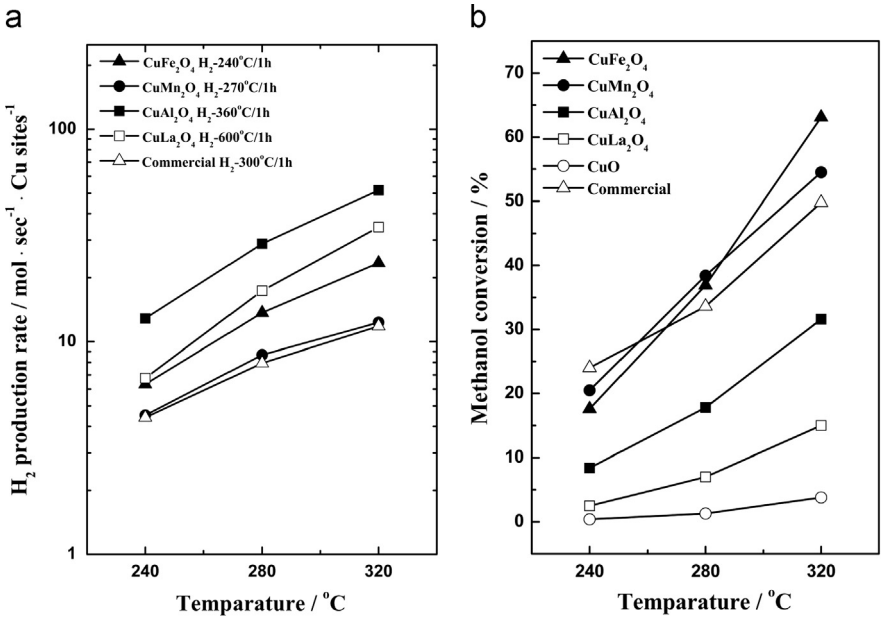

Fig. 8. H_2 production rate versus reaction temperature for steam reforming of methanol over the Cu-based spinel compounds, CuO and commercial catalyst after H_2 reduction in terms of [mol sec^{-1}Cu $sites^{-1}$] (a) and Methanol conversion over the Cu-based spinel compounds, CuO and commercial catalyst for SRM at different temperatures (b).

temperature. Formation of CO by reverse water–gas shift and direct methanol decomposition is to be avoided in methanol reforming to the greatest extent possible. As the B-site component, the CuO compound without metal oxide presented the highest CO selectivity and the lowest CO_2 selectivity, which was ascribable to the sintering of the active Cu particles that led to ready aggregation of the Cu particles during H_2 reduction treatment. This phenomenon in turn resulted in a loss of the Cu surface area and brought down the methanol conversion to less than ~4% at 320 °C. Furthermore, the results revealed that the reduced $CuAl_2O_4$ powders possessed the lowest CO selectivity value ranging from 0 to 1.05% and the highest CO_2 selectivity values from 100 to 98.95% with respect to the reaction temperature from 240 to 320 °C; both values were nearly the same as those of commercial catalyst. The CO selectivity values of the reduced $CuMn_2O_4$ and $CuFe_2O_4$ powders appeared to be very similar, ranging from ≈0.5% at 240 °C to ≈2% at 320 °C, while that of the reduced $CuLa_2O_4$ powders read 1.4 to 3.3% in the temperature range measured. The higher catalytic activity of the $CuAl_2O_4$ powders apparently contributed to its larger surface area.

Fig. 10 presents the XRD patterns of the reduced Cu-based spinel compounds after the SRM reaction. The diffraction patterns of the $CuMn_2O_4$, $CuFe_2O_4$ and $CuAl_2O_4$ samples showed nearly no variation, and the phase structures of Cu and MnO in the $CuMn_2O_4$ sample, those of Cu and Fe_3O_4 in the $CuFe_2O_4$ sample, and those of Cu and γ-Al_2O_3 in the $CuAl_2O_4$ sample remained unchanged after the SRM reaction. The stability of these species clearly indicates that all the MnO, Fe_3O_4 and γ-Al_2O_3 supports provided a higher thermal stability to hold the Cu particles. However, for the reduced $CuLa_2O_4$ sample, major phase of $La(OH)_3$ (JCPDS card #36-1481) was detected, in addition to the La_2O_3 and Cu species. Because La_2O_3 is hygroscopic and tends to form $La(OH)_3$ in a moist atmosphere, the TG/DSC (Thermal Gravimetry with Differential Scanning Calorimetry) results indicate the complete decomposition of

Table 2
Results of Cu particle measurement on surface, TOF value.

Catalyst	Adsorption sites [a] [10^{17} g-Cu]	Cu particles[a] Surface area from titration [m^2/g-Cu]	Cu dispersion[a] [%]	TOF[b] [s^{-1}]
$CuFe_2O_4$	11.6	17.0	2.6	119.5
$CuMn_2O_4$	37.8	61.9	9.5	69.7
$CuAl_2O_4$	6.4	14.6	2.2	327.6
$CuLa_2O_4$	2.4	5.8	0.9	289.3
CuO	2.1	0.9	0.1	27.0
Commercial Cat.	47.3	68.3	10.5	59.9

[a]Cu particle size, surface area and dispersion calculated from N_2O chemisorption at room temperature.
[b]Reaction temperature at 280 °C.

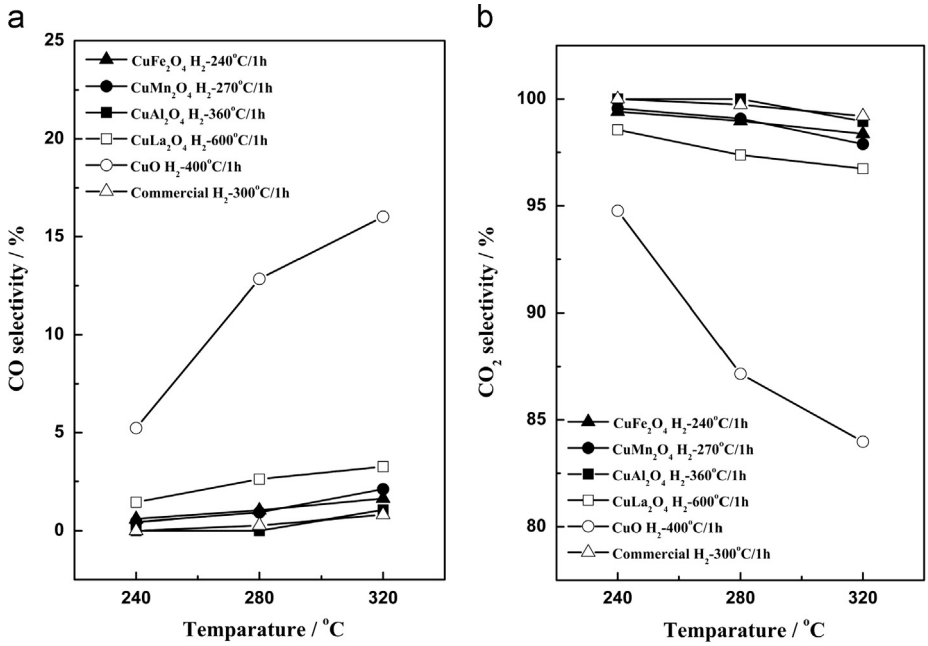

Fig. 9. Selectivity of CO_2 and CO versus reaction temperature of the Cu-based spinel compounds for steam reforming of methanol after SRM reaction.

hydrated lanthanum oxide above 750 °C [27–28]. La was thus found to easily adsorb the (OH) bonds and become hydrolyzed under a high temperature together with a high humidity and during the SRM reaction. On the other hand, the spinel structure of these series of Cu-based spinel compounds can be easily restored through reversible treatment in air at 1000 °C.

Taking into account of the overall results, the reduced $CuAl_2O_4$ powders show the best catalytic activity for SRM reaction (followed subsequently by the reduced $CuLa_2O_4$ powders, the reduced $CuFe_2O_4$ powders, and the reduced $CuMn_2O_4$ powders), which can be attributed to the formation of a large surface area marked with a porous structure generated by the reduction of $CuAl_2O_4$ and the nano-sized Cu particles homogenously precipitated on the γ-Al_2O_3 support. The results are different from those about the Cu-based spinel compounds for use in the steam reforming of dimethyl ether (DMESR) reported in the literature [29] which revealed that the catalytic activities of the $CuAl_2O_4$ and $CuMn_2O_4$ powders are inferior to that of the $CuFe_2O_4$ powders. It is also evident that the precipitation of nano-sized Cu particles on the support of porous γ-Al_2O_3 skeleton via the reduction of $CuAl_2O_4$ spinel compound appears to be an effective synthesis route for catalysts with high catalytic activity and thermal stability for SRM reaction.

4. Conclusions

Based on the results of this study, the reduction behaviors and morphological changes of Cu-based spinel compounds were found to depend strongly on the B-site component. After reduction treatment in H_2 atmosphere, the Cu-based spinel compounds were reduced to copper-oxide composites with precipitated copper nanoparticles. The catalytic performances with respect to (mol min^{-1} Cu-$site^{-1}$) for SRM of these

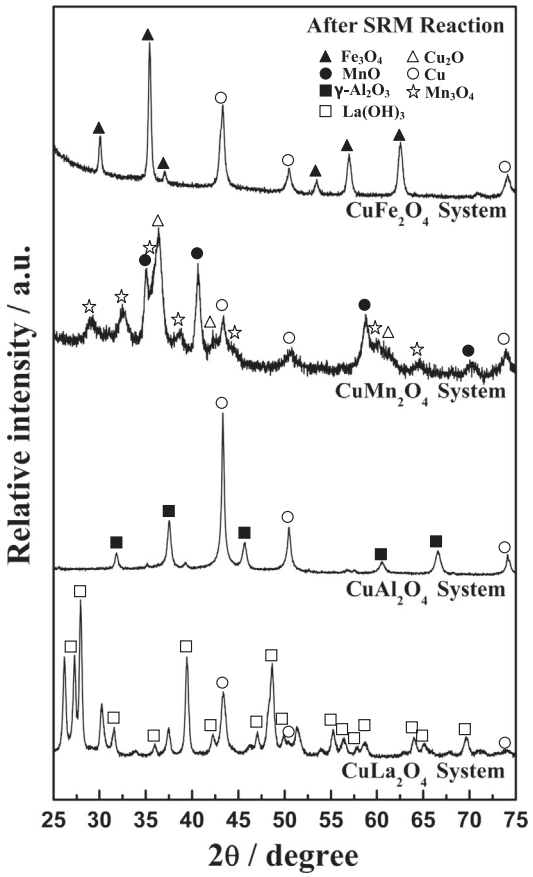

Fig. 10. XRD patterns of the Cu-based spinel compounds after SRM reaction.

copper-oxides composites were superior to those of conventional copper catalysts. These catalytic properties are ascribed to the interaction between copper nanoparticles and oxides. The present study demonstrates the potential of spinel oxides as a promising precursor for high-performance copper catalysts.

References

[1] B. Lindström, L.J. Pettersson, P.Govind Menon, Activity and characterization of Cu/Zn, Cu/Cr and Cu/Zr on γ-alumina for methanol reforming for fuel cell vehicles, Applied Catalysis A: General 234 (2002) 111–125.

[2] S. Patel, K.K. Pant, Activity and stability enhancement of copper–alumina catalysts using cerium and zinc promoters for the selective production of hydrogen via steam reforming of methanol, Journal of Power Sources 159 (2006) 139–143.

[3] S.D. Jones, H.E. Hagelin-Weaver, Steam reforming of methanol over CeO_2- and ZrO_2-promoted Cu–ZnO catalysts supported on nanoparticle Al_2O_3, Applied Catalysis B: Environmental 90 (2009) 195–204.

[4] H. Jeong, K.I. Kim, T.H. Kim, C.H. Ko, H.C. Park, I.K. Song, Hydrogen production by steam reforming of methanol in a micro-channel reactor coated with Cu/ZnO/ZrO_2/Al_2O_3 catalyst, Journal of Power Sources 159 (2006) 1296–1299.

[5] J. Agrell, H. Birgersson, M. Boutonnet, I. Melián-Cabrera, R.M. Navarro, J.L. G. Fierro, Production of hydrogen from methanol over Cu/ZnO catalysts promoted by ZrO_2 and Al_2O_3, Journal of Catalysis 219 (2003) 389–403.

[6] P.P.C. Udani, P.V.D.S. Gunawardana, H.C. Lee, D.H. Kim, Steam reforming and oxidative steam reforming of methanol over CuO–CeO_2 catalysts, International Journal of Hydrogen Energy 34 (2009) 7648–7655.

[7] P.H. Matter, D.J. Braden, U.S. Ozkan, Steam reforming of methanol to H_2 over nonreduced Zr-containing CuO/ZnO catalysts, Journal of Catalysis 223 (2004) 340–351.

[8] P.H. Matter, U.S. Ozkan, Effect of pretreatment conditions on Cu/Zn/Zr-based catalysts for the steam reforming of methanol to H_2, Journal of Catalysis 234 (2005) 463–475.

[9] Y. Tanaka, T. Utaka, R. Kikuchi, T. Takeguchi, K. Sasaki, K. Eguchi, Water gas shift reaction for the reformed fuels over Cu/MnO catalysts prepared via spinel-type oxide, Journal of Catalysis 215 (2003) 271–278.

[10] Y. Tanaka, T. Utaka, R. Kikuchi, K. Sasaki, K. Eguchi, Water gas shift reaction over Cu-based mixed oxides for CO removal from the reformed fuels, Applied Catalysis A: General 242 (2003) 287–295.

[11] Y. Tanaka, T. Takeguchi, R. Kikuchi, K. Eguchi, Influence of preparation method and additive for Cu–Mn spinel oxide catalyst on water gas shift reaction of reformed fuels, Applied Catalysis A: General 279 (2005) 59–66.

[12] J. Papavasiliou, G. Avgouropoulos, T. Ioannides, In situ combustion synthesis of structured Cu–Ce–O and Cu–Mn–O catalysts for the production and purification of hydrogen, Applied Catalysis B: Environmental 66 (2006) 168–174.

[13] J. Papavasiliou, G. Avgouropoulos, T. Ioannides, Combined steam reforming of methanol over Cu–Mn spinel oxide catalysts, Journal of Catalysis 251 (2007) 7–20.

[14] S. Kameoka, T. Tanabe, A.P. Tsai, Self-assembled porous nano-composite with high catalytic performance by reduction of tetragonal spinel $CuFe_2O_4$, Applied Catalysis A: General 375 (2010) 163–171.

[15] S. Kameoka, Mi. Okada, A.P. Tsai, Preparation of a novel copper catalyst in terms of the immiscible interaction between copper and chromium, Catalysis Letters 120 (2008) 252–256.

[16] J.W. Evans, M.S. Wainwright, A.J. Bridgewater, D.J. Young, On the determination of copper surface area by reaction with nitrous oxide, Applied Catalysis 7 (1983) 75–83.

[17] C.J.G. Van Der Grift, A.F.H. Wielers, B.P.J. Joghi, J. Van Beijnum, M. De Boer, M. Versluijs-Helder, J.W. Geus, Effect of the reduction treatment on the structure and reactivity of silica-supported copper particles, Journal of Catalysis 131 (1991) 178–189.

[18] S. Kameoka, T. Tanabe, A.P. Tsai, Spinel $CuFe_2O_4$: a precursor for copper catalyst with high thermal stability and activity, Catalysis Letters 100 (2005) 89–93.

[19] M.F. Luo, P. Fang, M. He, Y.L. Xie, In Situ XRD, Raman, and TPR Studies of CuO/Al_2O_3 Catalysts for CO Oxidation, Journal of Molecular Catalysis A: Chemical 239 (2005) 243–248.

[20] H. Yahiro, K. Nakaya, T. Yamamoto, K. Saiki, H. Yamaura, Effect of calculation temperature on the catalytic activity of copper supported on γ-alumina for the water–gas-shift reaction, Catalysis Communication 7 (2006) 228–231.

[21] Y. Kawamura, K. Yamamoto, N. Ogura, T. Katsumata, A. Igarashi, Preparation of Cu/ZnO/Al_2O_3 catalyst for a micro methanol reformer, Journal of Power Sources 150 (2005) 20–26.

[22] A.P. Tsai, M. Yoshimura, Highly active quasicrystalline Al–Cu–Fe catalyst for steam reforming of methanol, Applied Catalysis A: General 214 (2001) 237–241.

[23] M. Turco, G. Bagnasco, C. Cammarano, P. Senese, U. Costantino, M. Sisani, Cu/ZnO/Al_2O_3 catalysts for oxidative steam reforming of methanol: The role of Cu and the dispersing oxide matrix, Applied Catalysis B: Environmental 77 (2007) 46–57.

[24] C.J. Jiang, D.L. Trimm, M.S. Wainwright, Kinetic study of steam reforming of methanol over copper-based catalysts, Applied Catalysis A: General 93 (1993) 245–255.

[25] N. Shimoda, K. Faungnawakij, R. Kikuchi, T. Fukunaga, K. Eguchi, Catalytic performance enhancement by heat treatment of $CuFe_2O_4$ spinel and γ-alumina composite catalysts for steam reforming of dimethyl ether, Applied Catalysis A: General 365 (2009) 71–78.

[26] K. Eguchi, N. Shimoda, K. Faungnawakij, T. Matsui, R. Kikuchi, S. Kawashima, Transmission electron microscopic observation on reduction

process of copper–iron spinel catalyst for steam reforming of dimethyl ether, Applied Catalysis B: Environmental 80 (2008) 156–167.

[27] L. Gao, G. Sun, S. Kawi, A study on methanol steam reforming to CO_2 and H_2 over the La_2CuO_4 nanofiber catalyst, Journal of Solid State Chemistry 181 (2008) 7–13.

[28] P.P. Fedorov, M.V. Nazarkin, R.M. Zakalyukin, On Polymorphism and Morphotropism of Rare Earth Sesquioxides, Crystallography Reports 47 (2002) 281–286.

[29] K. Faungnawakij, N. Shimoda, T. Fukunaga, R.i Kikuchi, K. Eguchi, Cu-based spinel catalysts CuB_2O_4 (B = Fe, Mn, Cr, Ga, Al, $Fe_{0.75}Mn_{0.25}$) for steam reforming of dimethyl ether, Applied Catalysis A: General 341 (2008) 139–145.

[30] G.C. Chinchen, C.M. Hay, H.D. Vandervell, K.C. Waugh, The measurement of copper surface areas by reactive frontal chromatography, Journal of Catalysis 103 (1987) 79–86.